Dual-polarized multiplexed meta-holograms utilizing coding metasurface

Chunsheng Guan, Jian Liu, Xumin Ding, Zhuochao Wang, Kuang Zhang, Haoyu Li, Ming Jin, Shah Nawaz Burokur, Qun Wu

Research article

Chunsheng Guan, Jian Liu, Xumin Ding*, Zhuochao Wang, Kuang Zhang*, Haoyu Li, Ming Jin, Shah Nawaz Burokur* and Qun Wu

Dual-polarized multiplexed meta-holograms utilizing coding metasurface

https://doi.org/10.1515/nanoph-2020-0237
Received April 16, 2020; accepted June 14, 2020; published online July 3, 2020

Abstract: In this paper, a novel method is proposed to achieve two distinct information channels by simultaneously manipulating both the transmitted cross- and co-polarized components of a 1-bit coding metasurface under linearly polarized incidence. Compared to previously demonstrated incidence-switchable or position multiplexed holograms, our proposed coding meta-hologram can simultaneously project two independent holographic images without inevitable change of the incidence state and can at the same time also avoid crosstalk between different channels. Moreover, the orientation of the double-layered split ring (SR) apertures is specially designed to be 45° or 135° to achieve identical multiplexed functionality for both *x*-polarized and *y*-polarized incidences. The proof-of-concept experimental demonstrations present total transmittance efficiency above 30% for the dual linearly polarized incidences at 15 GHz, and good imaging performances with 53.98%/48.18% imaging efficiency, 1.55%/1.46% RMSE, and 29.9/28.72 peak signal-to-noise ratio for the cross-/co-polarized channels under *y*-polarized incidence, and 47.27%/45.75% imaging efficiency, 1.55%/1.43% RMSE, and 18.74/25.93 peak signal-to-noise ratio under *x*-polarized incidence, demonstrating great potential of the proposed multiplexed coding meta-hologram in practical applications such as data storage and information processing.

Keywords: coding metasurface; dual-polarized; meta-holograms; multiplexed.

1 Introduction

Holography is one of the most promising imaging techniques to record and reconstruct full wave information of objects [1]. Traditional holograms can be generated either by interference of a reference beam with the scattered beam from a real object, or by using numerical computation to calculate the phase information into surface structures [2–4]. Metasurfaces, composed of arrays of artificially designed planar subwavelength-scaled scatterers, are two-dimensional analogues of metamaterials [5–10]. Due to their extraordinary capability in tailoring wavefronts, numerous applications of metasurfaces have been proposed, such as anomalous reflectors/refractors [11, 12], metalenses [13, 14], orbital angular momentum (OAM) generators [15, 16], metagratings [17, 18] and multifunctional devices [19, 20], to name a few. Metasurfaces also provide an alternative approach to achieve high quality holographic imaging [20–30]. Particularly, in microwave regime, the holographic metasurface offers a mechanism to achieve the accurate and elaborate control of electromagnetic near field, which will be profitable to short-range communication systems, detection, security, data storage, and information processing [31–33]. Compared to conventional holograms, metasurface can not only provide unprecedented spatial resolution, low noise and high precision of the reconstructed images, but also establish the feasibility of multiplexed hologram without introducing distortion in the reconstruction [20, 34–41].

Chunsheng Guan and Jian Liu: These authors contributed equally to this work.

***Corresponding authors: Xumin Ding**, Advanced Microscopy and Instrumentation Research Center, Harbin Institute of Technology, Harbin 150080, China; Department of Microwave Engineering, Harbin Institute of Technology, Harbin 150001, China, E-mail: xuminding@hit.edu.cn; **Kuang Zhang**, Department of Microwave Engineering, Harbin Institute of Technology, Harbin 150001, China, E-mail: zhangkuang@hit.edu.cn; and **Shah Nawaz Burokur**, LEME, UPL, Univ Paris Nanterre, F92410 Ville d'Avray, France, E-mail: sburokur@parisnanterre.fr

Chunsheng Guan and Zhuochao Wang: Advanced Microscopy and Instrumentation Research Center, Harbin Institute of Technology, Harbin 150080, China; Department of Microwave Engineering, Harbin Institute of Technology, Harbin 150001, China

Jian Liu and Haoyu Li: Advanced Microscopy and Instrumentation Research Center, Harbin Institute of Technology, Harbin 150080, China

Ming Jin and Qun Wu: Department of Microwave Engineering, Harbin Institute of Technology, Harbin 150001, China

In general, there are several basic techniques for multiplexed hologram, including multicolor [34, 35], polarization [20, 36–38], incidence angle [39], OAM mode [40] and position [39, 41]. The multicolor multiplexing is based on independent record and reconstruction of the phase and amplitude information on different color components. The principle of polarization multiplexing relies on the use of polarization state as an additional degree of freedom. Previously published works have reported the implementation of the polarization-switchable multiplexed hologram with two distinct patterns for any pair of orthogonal states of polarization: linear, circular or elliptical. Nevertheless, this kind of polarization multiplexing can control only one polarization part in the transmitted or reflected field and leaves the other polarization part unchanged, which results in the waste and loss of energy and channel carried by the neglected polarization. The OAM mode multiplexing is realized by utilizing strong OAM selectivity as an information carrier offered by meta-holograms consisting of GaN nano-pillars with discrete spatial frequency distributions. For the incidence angle multiplexing, different holograms can be generated when the wave illuminates at different angles. However for the aforementioned methods, multiplexed holograms can only be switched by changing the incidence frequency, polarization, OAM mode or angle. The position multiplexing offers a simple method to simultaneously project multiple images by superposing the phase information of images at different angles or distances on one metasurface, but usually suffers from strong crosstalk between different images. How to realize multiplexed hologram without inevitable change of incident state and at the same time avoiding crosstalk is still a big challenge and has not been fully explored.

Here, a transmission-type 1-bit coding metasurface is proposed for multiplexed hologram in microwave region. Compared to previously demonstrated incidence-switchable or position multiplexing, our proposed 1-bit coding meta-hologram can simultaneously project two separated images based on two orthogonal linear polarization states of the transmitted wave under linearly polarized incidence. Since the holographic information in the two channels are encoded into orthogonal transmitted polarizations, which can be independently controlled utilizing the 1-bit coding metasurface, this kind of method can also avoid crosstalk between different channels. The proposed metasurface is constructed by double-layered transmissive SR subwavelength elements, which enable to manipulate both transmitted cross- and co-polarized components under specific linearly polarized incidence. By elaborately designing the element width and gap opening of the constituting SR apertures, a group of four digital elements ("0 + 0" to "1 + 1") is extracted to construct the 1-bit coding meta-hologram. The digits before and after the "+" indicate the operational status of the transmitted cross- and co-polarized component, and "0" and "1" correspond to phase "0" and "π", respectively [42, 43]. The orientation of the SR apertures is specially designed to be 45° or 135°. In such case, identical multiplexed hologram can be achieved under both x-polarized and y-polarized incidences. A modified weighted Gerchberg-Saxton (GSW) algorithm is implemented to calculate the interfacial phase distribution. The 1-bit coding meta-hologram is formed by arranging the digital elements based on the 1-bit coding maps discretized from the calculated phase distribution. Experimental verifications performed on a fabricated prototype agree qualitatively with the theoretical predictions and numerical simulations, indicating the feasibility and high imaging quality of the proposed 1-bit dual-polarized multiplexed coding meta-hologram.

2 Design of the coding elements

The schematic representation of the proposed 1-bit coding meta-hologram is depicted in Figure 1. The key step to realize the proposed multiplexed hologram is to elaborately design meta-atoms capable of producing separately adjustable phase response of transmitted components for orthogonal polarization states. A double-layer metallic unit structure is proposed to construct the metasurface, in which two symmetric SR apertures are spaced by a F4B dielectric substrate, as shown in Figure 2a. The relative permittivity and loss tangent of the F4B substrate are $\varepsilon_r = 3$ and $\tan\delta = 0.0015$, respectively, and the thickness of the substrate is $t = 1.5$ mm, which is only $0.075\,\lambda_0$ at the operating frequency of 15 GHz. Other geometrical parameters shown in Figure 2a are periodicity $p = 8$ mm, outer radius $r = 7$ mm, and element width w and gap opening angle θ are used as variables. As shown in Supplementary material S1, the choice of periodicity p is made as a tradeoff between periodic conditions and spatial resolution of the phase profile. A comprehensive parametric study on w and θ is implemented to achieve desired coding elements exposing arbitrary 1-bit transmission phase of 0° and 180° for both transmitted cross- and co-polarized components. Four coding elements are extracted from this process, as shown in Figure 2b. With an orientation of 45°, π phase shift of the co-polarized component can be achieved by changing element width and gap opening angle of SR apertures, as shown in Figure 2b ("0 + 0" and "0 + 1"). Another π phase shift of the cross-polarized component can be realized by rotating the two elements from 45° to 135° [5],

as shown in Figure 2b ("1 + 0" and "1 + 1"). Since the orientation of the SR apertures are specially designed to be 45° or 135°, the transmittance responses of the cross- and co-polarized components of *x*-polarized and *y*-polarized incidences are totally identical, providing the dual-polarized functionality for the meta-hologram. As discussed above, for our proposed multiplexed 1-bit coding meta-hologram, only two elements needs to be designed by modulating two parameters, the other two elements can be easily realized by rotating the obtained ones, which greatly simplifies the design process.

The four coding elements are characterized by applying unit cell boundary conditions in *x*- and *y*-directions under incidence of *x*- or *y*-polarized plane waves. The transmission amplitude and phase spectrum of the designed coding elements are depicted in Figure 2c–f. As it can be seen from Figure 2c and e, the transmission amplitude of the coding elements in each column in Figure 2b ("0 + 0" and "1 + 0", "0 + 1" and "1 + 1") is identical, and the transmission amplitude of the four coding elements is around 0.4 for both cross- and co-polarized components at 15 GHz. Figure 2d shows that the phase difference between "0 + 0" and "1 + 0" (or "0 + 1" and "1 + 1") is π for the transmitted cross-polarized component at 15 GHz, and Figure 2f shows that there is a π phase difference between "0 + 0" and "0 + 1" (or "1 + 0" and "1 + 1") for the transmitted co-polarized component, providing a new degree of freedom to have independent phase state in each cross- and co-polarized component sharing the same aperture. The proposed design can also be scaled up for multi-bit operation by using a multilayer structure with higher resonance order [44]. However, since there are more parameters to be optimized, the multi-layer structure will greatly increase the design complication. Moreover, it also requires more simulation time and storage capacity to analyze the interactions between the different layers. Thus, here a 1-bit coding metasurface is designed, which not only achieves good imaging performance, but also greatly simplifies the design process.

3 Design of the coding meta-hologram

To design the dual-channel coding meta-hologram in Figure 1, the coding map of each image can be separately derived using the modified WGS retrieval algorithm [45, 46]. To consider high resolution, the imaging plane here is designed to be 4λ away from the meta-hologram, which is an acceptable distance for lens antennas and short-range communications [33, 47–50]. A metasurface with focal distance in the radiative near field can also find applications in high numerical aperture (NA) lenses to achieve high imaging resolution at millimeter wavelengths [51] or higher frequencies [52]. Due to the limited focal distances with respect to the working wavelength, the Fraunhofer diffraction of optical regime is modified by Green function [20]. The method is to select ideal point sources as virtual sources and place them at pre-designed hotspots. Considering there are N hotspots located at (x_n, y_n, z_n) ($n = 1$ to N), the phase delay at the position of each coding element $\phi(x_m, y_m, z_m)$ ($m = 1$ to M) can be retrieved by superposing the electromagnetic field generated by all the virtual sources described by Green function. Accordingly, the reconstructed electric field is converged to the predesigned hotspots. In order to keep uniform intensity distribution among hotspots, a weighted factor w_m is introduced to reduce intensity difference among N hotspots. An iterative

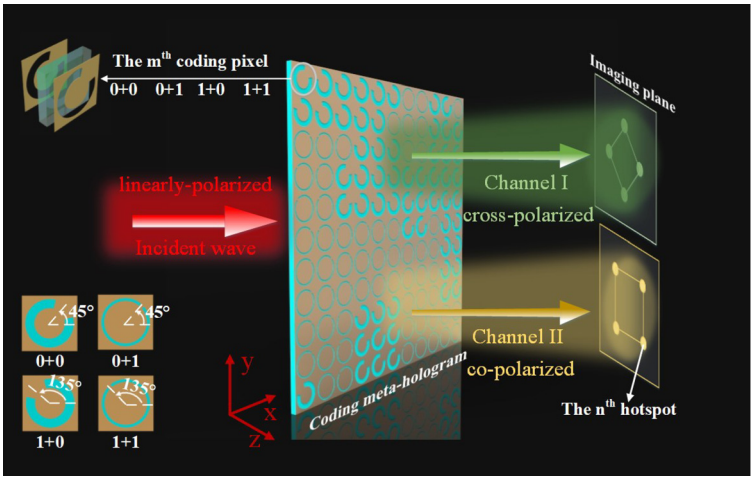

Figure 1: Schematic diagram of the coding elements as well as the proposed coding meta-hologram creating two different information channels based on the transmitted cross- and co-polarized components upon illumination of normally incident linearly-polarized plane wave. Two different images (a rhombus and a squares, here) can be simultaneously projected in the two near-field channels.

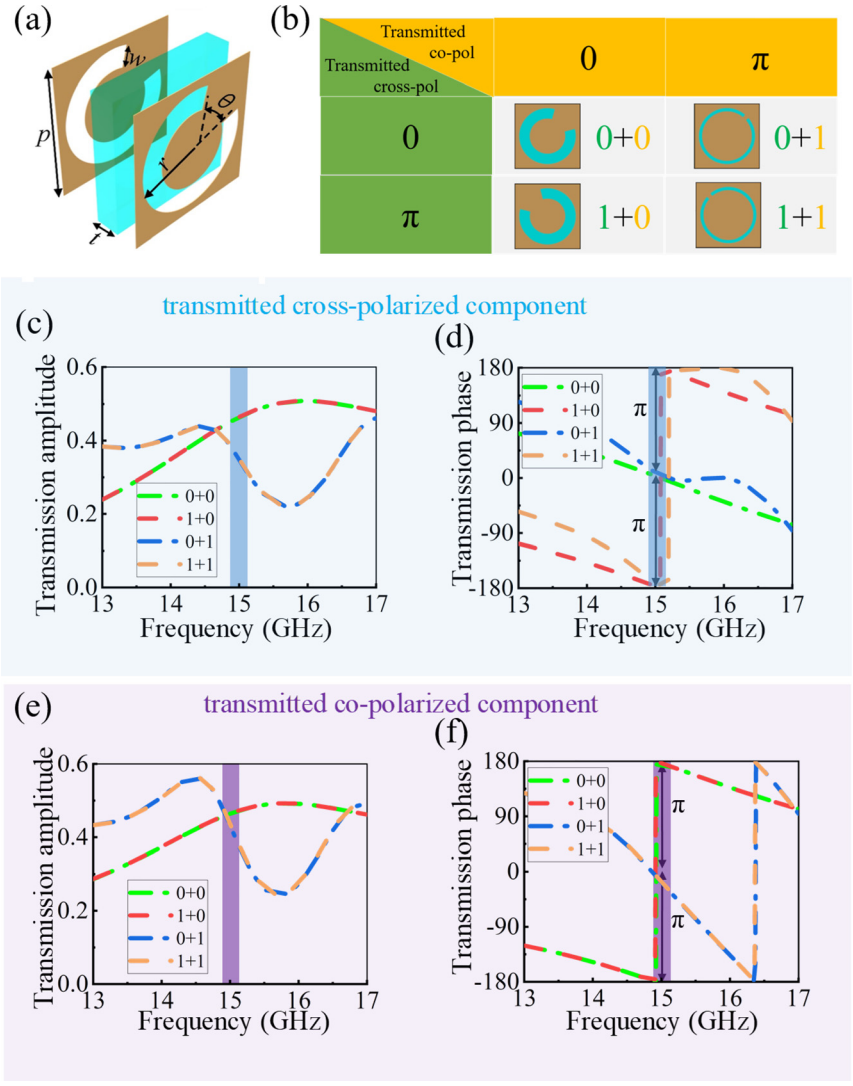

Figure 2: (a) Schematic view of the coding element. (b) Details of the designed four coding elements. Phase response along the horizontal and vertical axes indicates the operational state of transmitted co- and cross-polarized components of the coding elements. (c) and (e) Transmission amplitude spectra of all four coding elements for the transmitted cross- and co-polarized component, respectively. (d) and (f) Transmission phase spectra of all four coding elements for the transmitted cross- and co-polarized component, respectively.

procedure between the holography imaging and meta-hologram is proposed to obtain the uniform intensity profile of the target image as follows:

$$\phi_m^p = \arg\left(\sum_{n=1}^{N} \frac{e^{ikr_m^n}}{r_m^n} \frac{w_n^p E_n^{p-1}}{|E_n^{p-1}|}\right) \tag{1}$$

$$E_n^p = \sum_{n=1}^{M} \frac{e^{-ikr_m^n + i\phi_m^p}}{r_m^n} \tag{2}$$

$$w_n^p = w_n^{p-1} \frac{\sum_{n=1}^{N} |E_n^{p-1}|}{N|E_n^{p-1}|} \tag{3}$$

where ϕ_m is defined as the phase shift of the mth ($m = 1$ to M) coding element and E_n denotes the electric field intensity of the nth ($n = 1$ to N) hotspots. r_m^n is the distance between mth coding element and nth hotspot and superscript p represents the pth iterative step. According to Equations (2) and (4), the weight factor w_m is adjusted step by step until the least mean square error between the target and the reconstructed image becomes less than a predesigned threshold. Particularly, the initial condition is set as:

$$w_n^0 = 1, \quad \phi_m^0 = \frac{2\pi m}{M} \tag{4}$$

Once the phase distributions of each channel are obtained based on the modified WGS algorithm, the calculated phase distributions are discretized to be 0 and π, and represented by code "0" and "1", respectively. In this way, the phase information of each cross- and co-polarized channel can be described by the 1-bit coding maps, as shown in Figure 3a,e. Then, the multiplexed 1-bit coding meta-hologram can be constructed by superimposing the two obtained coding maps based on the coding rule of Figure 2b.

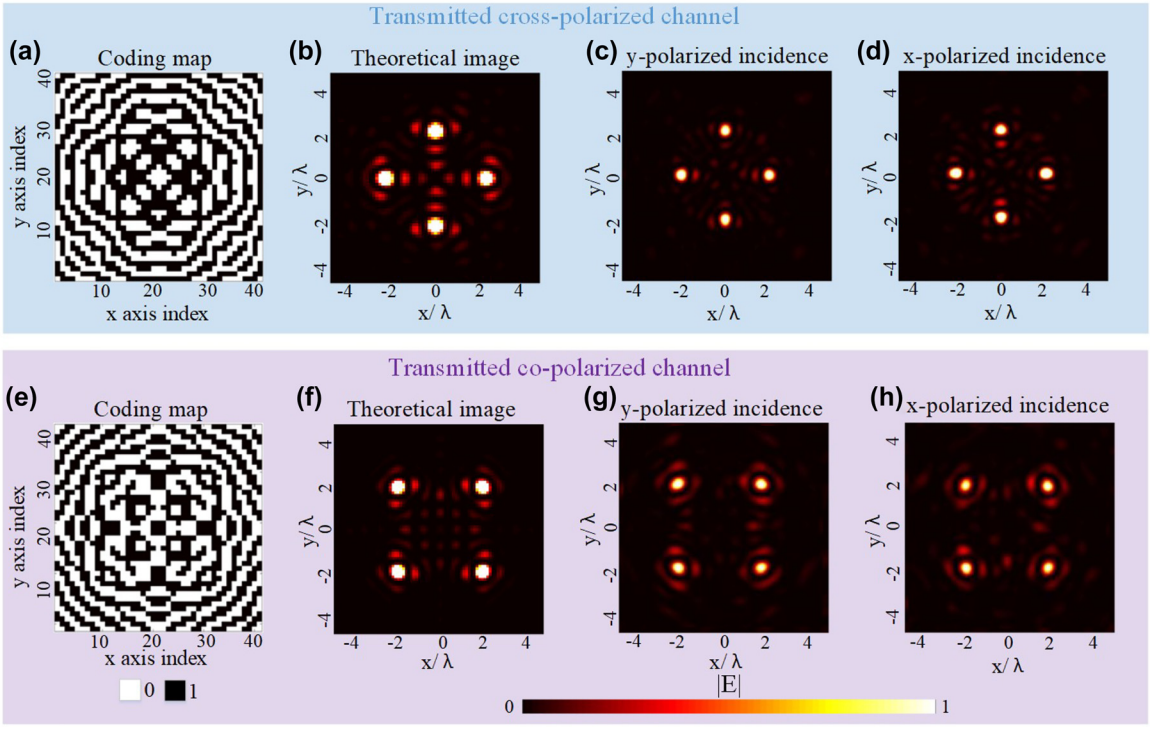

Figure 3: Coding maps and theoretical and simulated results of the electric field intensity distributions: (a)–(d) cross-polarized transmission channel projecting the image of a "rhombus" and (e)–(h) co-polarized transmission channel projecting the image of a "square".

4 Results and discussion

To demonstrate our proposed method, a 1-bit coding meta-hologram is designed and simulated to project "rhombus" and "square" images in the transmitted near-field cross- and co-polarized channels, respectively. In the near field imaging simulation, the metasurface is subjected to open boundary conditions along *x*- and *y*-axes, and illuminated by an *x*- or *y*-polarized normally incident wave. Figure 3b and f shows the theoretically calculated results, Figure 3c and g presents the simulated results of the cross- and co-channels under *y*-polarized incidence, and Figure 3d and h presents the simulated results of the cross- and co-channels under *x*-polarized incidence. Since the imaging plane is in the radiative near-field region, the longitudinal polarized (E_z) component also exists, as discussed in detail in Supplementary material S2. It is obvious that the images in the cross- and co-polarized channels are identical for *x*- and *y*-polarized incidences, and the simulated results show great agreement with the theoretical designs. As shown in Figure 3c and 3g (or Figure 3d and 3h), the hotspots generated in the two channels are located at different positions. Thus in near-field communication, receivers with different polarization state can be placed at the corresponding hotspots to retrieve information transmitted in the two channels.

To further verify the performances of the proposed 1-bit coding meta-hologram, a sample consisting of 41×41 unit cells with an overall size of 328×328 mm is fabricated using conventional printed circuit board (PCB) technique, as shown by the photography in Figure 4a. Measurements are performed using a near field scanning system, as illustrated by the experimental setup schematic in Figure 4b. A feeding horn antenna is placed far away from the metasurface to ensure the incident quasi-plane wave at 15 GHz. A fiber optic active antenna is used as field probe to measure the electric field distribution in the transmitted region. Both the feeding horn antenna and the field sensing probe are connected to a vector network analyzer (VNA) to measure the transmission coefficients of the *x*- and *y*-polarized components.

Figure 4c–f shows the measured holographic images of transmitted cross- and co-polarized channels at a distance of 80 mm (4λ) at 15 GHz under *x*-polarized and *y*-polarized incidences, highlighting well four hotspots with nearly uniform intensities in good accordance with the theoretical predictions and simulated results. The slight intensity variation among the four hotspots in Figure 4 mainly comes from the slight off-axis deviation of non-planar wavefronts of the incident field distribution from the feeding horn antenna across the metasurface, compared to normally incident ideal

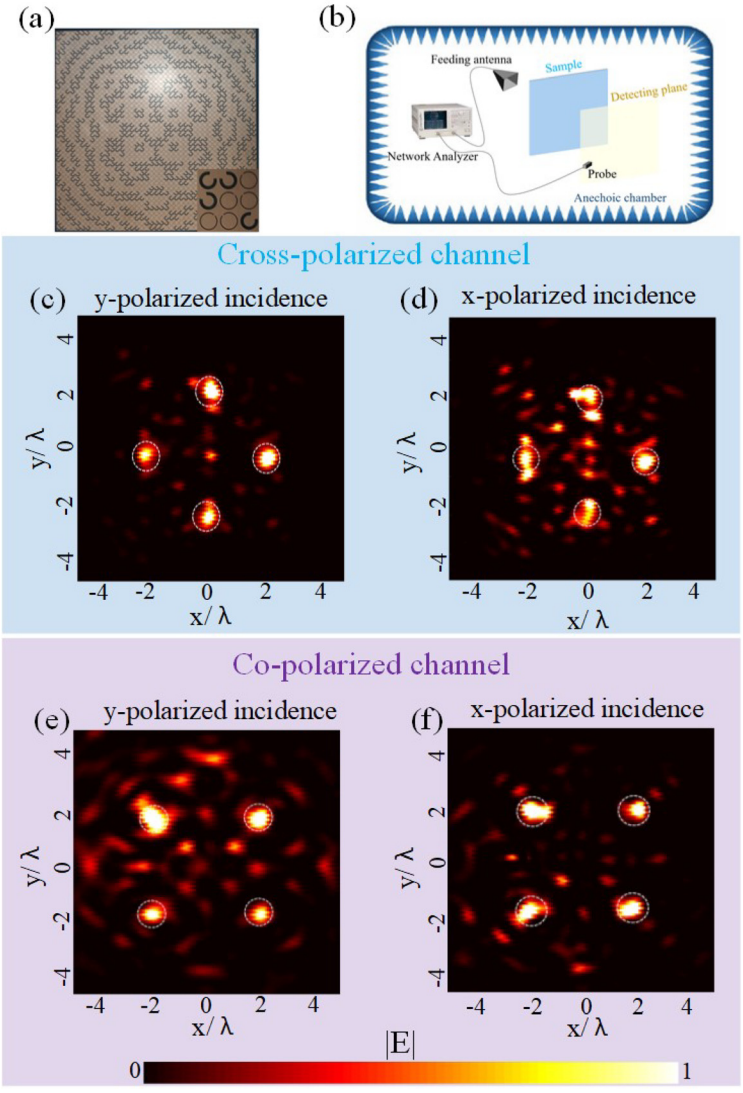

Figure 4: (a) Photography of fabricated sample. (b) Illustration of experimental setup. (c) and (d) Measured holographic "rhombus" images of the cross-polarized channel under *y*- and *x*-polarized incidence, respectively. (e) and (f) Measured holographic "square" images of the co-polarized channel under *y*- and *x*-polarized incidence, respectively.

planar wavefronts considered in simulations. Four parameters are adopted here to evaluate the imaging quality of the holographic images. The transmittance efficiency, which characterizes the transmission characteristic of the proposed metasurface, is defined as the total intensity of the wave passing through the metasurface referenced to the incident intensity on a surface of the same size [53, 54]. The imaging efficiency, describing the ability to transform the incident energy into the designated points, is calculated by the energy concentrated in the preset hotspots referenced to the total transmitted energy in the measured plane [55]. The root-mean-square error (RMSE), describing the deviations between the measured intensity ratios and theoretical values, is used to evaluate the manipulation ability of energy allocation of the hotspots [22]. And finally, the peak signal-to-noise ratio (PSNR) also used and is defined as the ratio between peak intensity in the image to the standard deviation of the background noise [56, 57]. Under *y*-polarized incident wave, the transmittance efficiency is measured to be respectively 12.1 and 18.5% for transmitted cross- and co-polarized component, and the total transmittance is found to be 30.6%. The imaging efficiency extracted from experimental data is calculated to be as high as 53.98 and 48.18% for the transmitted cross- and co-polarized channel, respectively. The measured RMSE reaches 1.55 and 1.46%, respectively, indicating a little deviation between theoretical design and measurement when the incident energy is transformed to the desired hotpots equally. Moreover, the PSNR is found to be 29.9 and 28.72 for the channels, which further verifies the superior image quality compared to previously reported metasurface holograms in microwave region [21, 23]. For *x*-polarized incidence, the measured results show good imaging quality with 15.6%/17.7% transmittance efficiency, 47.27%/45.75% imaging efficiency, 1.55%/1.43% RMSE and

18.74/25.93 PSNR for the cross- and co-polarized channels, respectively.

As shown in Figure 4, there is a small amount of diffracted fields near the four focal points. These higher order harmonic components in the images are induced by the EM wave that propagates through the metasurface. During illumination, higher order harmonics of the fundamental diffracted light patterns are generated within the fields near the four focal points. To restrain the emerging unnecessary information and improve the hologram, a threshold-value filtering indicator can be applied during the post processing operations. Furthermore, to improve the holographic imaging and achieve a better image quality, spatial denoising operation algorithm that can enhance the spatial resolution and remains a Haze like background, may be included in this post-processing model to reduce the random noise thoroughly. Although our proposed 1-bit coding metasurface has shown good imaging quality predicted by theoretical calculations and full wave simulations for dual linear polarizations, the imaging efficiency can be further improved by using a high-efficiency transmissive metasurface or reflective metasurface. An all-dielectric transmissive metasurface is usually used at optical frequencies, which enables avoiding high reflection effect and Ohmic losses of metal parts to achieve high transmission efficiency [58]. At microwave frequencies, the high efficiency transmissive metasurface can be achieved by utilizing multi-layer metal-dielectric structure [15]. High-efficiency reflective metasurface is widely used both at optical and microwave frequencies [25, 59]. Backed by the metal ground plane, the reflective metasurface can theoretically achieve 100% reflection efficiency. Moreover, based on the physical property of reciprocity, such holographic metasurface can find applications in the design of metalenses for antenna directivity enhancement with arbitrary feeding configuration including feed number and location [47], as detailed in Supplementary material S3. The polarization state of output beam can also be switched by changing the polarization of the radiating elements at the position of the hotspots, providing another degree of freedom for the antenna metalens design. Compact integrated source-metasurface systems can be considered in the future through the use of planar Fabry–Perot cavity antenna as illuminating source [60].

5 Conclusion

In conclusion, a dual-polarized multiplexed 1-bit coding meta-hologram with an ultrathin thickness of 0.075 λ_0 is realized using four simple coding elements, and it is experimentally validated in the microwave region. By simultaneously manipulating both the transmitted cross- and co-polarized components under linearly polarized incidences, the coding meta-hologram judiciously opens two near-field channels based on the polarization states of the transmitted wave, which can independently project two arbitrary images at the same time without inevitable change in the state of the incident wave. Moreover, the proposed meta-hologram can operate under both *x*- and *y*-polarized orthogonal incidences. The simulated and measured images show good agreement with the theoretical predictions, and the experimental measurements achieve good imaging performances in terms of total transmittance efficiency, imaging efficiency, RMSE, and peak signal-to-noise ratio for the cross- and co-polarized channels under both *x*- and *y*-polarized linearly polarized incidences. Such ultrathin, dual-polarized and multiplexed transmission-type meta-hologram may find practical applications in information storage/display, polarimetric imaging and holographic data encryption.

Acknowledgments: This paper is supported by the National Natural Science Foundation of China (Grant no. 61701141).
Author contribution: All the authors have accepted responsibility for the entire content of this submitted manuscript and approved submission.
Research funding: This paper is supported by the National Natural Science Foundation of China (Grant no. 61701141).
Conflict of interest: The authors declare no conflicts of interest.

References

[1] M. K. Kim, "Principles and techniques of digital holographic microscopy," *SPIE Rev.*, vol. 1, 2010, Art no. 018005.
[2] D. Gabor, "A new microscopic principle," *Nature*, vol. 161, pp. 777, 1948.
[3] U. Schanars, C. Falldorf, J. Watson, and W. Jueptner. *Digital Holography and Wavefront Sensing: Principles, Techniques and Applications*, Berlin Heidelberg, Germany, Springer-Verlag, 2015.
[4] B. R. Brown, and A. W. Lohmann, "Complex spatial filtering with binary masks," *Appl. Opt.*, vol. 5, pp. 967–969, 1966.
[5] N. Yu, P. Genevet, M. A. Kats, et al., "Light propagation with phase discontinuities: generalized laws of reflection and refraction," *Science*, vol. 334, pp. 333–337, 2011.
[6] N. Yu, and F. Capasso, "Flat optics with designer metasurfaces," *Nat. Mater.*, vol. 13, pp. 139–150, 2014.
[7] X. Ding, F. Monticone, K. Zhang, et al., "Ultrathin Pancharatnam–Berry metasurface with maximal cross-polarization efficiency," *Adv. Mater.*, vol. 27, pp. 1195–1200, 2015.

[8] A. V. Kildishev, A. Boltasseva, and V. M. Shalaev, "Planar photonics with metasurfaces," *Science*, vol. 339, pp. 1232009, 2013.
[9] M. R. Akram, M. Q. Mehmood, X. Bai, R. Jin, M. Premaratne, and W. Zhu, "High efficiency ultrathin transmissive metasurfaces," *Adv. Opt. Mater.*, vol. 7, pp. 1801628, 2019.
[10] M R. Akram, G. Ding, K. Chen, Y. Feng, and W. Zhu, "Ultrathin single layer metasurfaces with ultra-wideband operation for both transmission and reflection," *Adv. Mater.*, vol. 32, pp. 1907308, 2020.
[11] S. Sun, K. Y. Yang, C. M. Wang, et al., "High-efficiency broadband anomalous reflection by gradient meta-surfaces," *Nano Lett.*, vol. 12, pp. 6223–6229, 2012.
[12] Y. Yuan, K. Zhang, X. Ding, B. Ratni, S. N. Burokur, and Q. Wu, "Complementary transmissive ultra-thin meta-deflectors for broadband polarization-independent refractions in the microwave region," *Photonics Res.*, vol. 7, pp. 80–88, 2019.
[13] F. Aieta, P. Genevet, M. A. Kats, et al., "Aberration-free ultrathin flat lenses and axicons at telecom wavelengths based on plasmonic metasurfaces," *Nano Lett.*, vol. 12, pp. 4932–4936, 2012.
[14] S. Wang, P. C. Wu, V. C. Su, et al., "A broadband achromatic metalens in the visible," *Nat. Nanotechnol.*, vol. 13, p. 227, 2018.
[15] K. Zhang, Y. Yuan, X. Ding, B. Ratni, S. N. Burokur, and Q. Wu, "High-efficiency metalenses with switchable functionalities in microwave region," *ACS Appl. Mater. Interfaces*, vol. 11, pp. 28423–28430, 2019.
[16] M. Q. Mehmood, S. Mei, S. Hussain, et al., "Visible-frequency metasurface for structuring and spatially multiplexing optical vortices," *Adv. Mater.*, vol. 28, pp. 2533–2539, 2016.
[17] V. Popov, F. Boust, and S. N. Burokur, "Constructing the near field and far field with reactive metagratings: study on the degrees of freedom," *Phys. Rev. Appl.*, vol. 11, 2019, Art no. 024074.
[18] A. Epstein, and O. Rabinovich, "Unveiling the properties of metagratings via a detailed analytical model for synthesis and analysis," *Phys. Rev. Appl.*, vol. 8, 2017, Art no. 054037.
[19] A. Arbabi, Y. Horie, M. Bagheri, and A. Faraon, "Dielectric metasurfaces for complete control of phase and polarization with subwavelength spatial resolution and high transmission," *Nat. Nanotechnol.*, vol. 10, pp. 937, 2015.
[20] D. Wen, F. Yue, G. Li, et al., "Helicity multiplexed broadband metasurface holograms," *Nat. Commun.*, vol. 6, p. 8241, 2015.
[21] C. Guan, Z. Wang, X. Ding, et al., "Coding Huygens' metasurface for enhanced quality holographic imaging," *Opt. Express*, vol. 27, pp. 7108–7119, 2019.
[22] Z. Wang, X. Ding, K. Zhang, et al., "Huygens metasurface holograms with the modulation of focal energy distribution," *Adv. Opt. Mater.*, vol. 6, pp. 1800121, 2018.
[23] Y. Wang, C. Guan, Z. Wang, et al., "Multi-focus hologram utilizing Pancharatnam–Berry phase elements based metamirror," *Opt. Lett.*, vol. 44, pp. 2189, 2019.
[24] J. Scheuer, and Y. Y. Holography, "Metasurfaces make it practical," *Nat. Nanotechnol.*, vol. 10, pp. 296, 2015.
[25] G. Zheng, H. Mühlenbernd, M. Kenney, G. Li, T. Zentgraf, and S. Zhang, "Metasurface holograms reaching 80% efficiency," *Nat. Nanotechnol.*, vol. 10, pp. 308, 2015.
[26] X. Ni, A. V. Kildishev, and V. M. Shalaev, "Metasurface holograms for visible light," *Nat. Commun.*, vol. 4, pp. 2807, 2013.
[27] W. Qiu, X. Zhang, E. Plum, et al., "Polarization and frequency multiplexed terahertz meta-holography," *Adv. Opt. Mater.*, vol. 5, pp. 1700277, 2017.
[28] Z. Huang, L. M. Daniel, and R. S. David, "Polarization-selective waveguide holography in the visible spectrum," *Opt. Express*, vol. 27, pp. 35631–35645, 2019.
[29] Z. Huang, L. M. Daniel, and R. S. David, "Out-of-plane computer-generated multicolor waveguide holography," *Optica*, vol. 6, pp. 119–124, 2019.
[30] Z. Huan, C. Zhang, J. Guo, S. Liu, X. Chen, and Y. Zhang, "Metasurface hologram for multi-image hiding and seeking," *Phys. Rev. Appl.*, vol. 12, 2019, Art no. 054011.
[31] L. Li, T. J. Cui, W. Ji, et al., "Electromagnetic reprogrammable coding-metasurface holograms," *Nat. Commun.*, vol. 8, pp. 197, 2017.
[32] L. Li, Y. Shuang, Q. Ma, et al., "Intelligent metasurface imager and recognizer," *Light Sci. Appl.*, vol. 8, pp. 97, 2019.
[33] X. Wan, Q. Zhang, T. Y. Chen, et al., "Multichannel direct transmissions of near-field information," *Light Sci. Appl.*, vol. 8, pp. 60, 2019.
[34] W. Wan, J. Gao, and X. Yang, "Full-color plasmonic metasurface holograms," *ACS Nano*, vol. 10, pp. 10671–10680, 2016.
[35] X. Li, L. Chen, Y. Li, et al., "Multicolor 3D meta-holography by broadband plasmonic modulation," *Sci. Adv.*, vol. 2, 2016, Art no. e1601102.
[36] W. T. Chen, K. Y. Yang, C. M. Wang, et al., "High-efficiency broadband meta-hologram with polarization-controlled dual images," *Nano Lett.*, vol. 14, pp. 225, 2014.
[37] J. P. B. Mueller, N. A. Rubin, R. C. Devlin, B. Groever, and F. Capasso, "Metasurface polarization optics: independent phase control of arbitrary orthogonal states of polarization," *Phys. Rev. Lett.*, vol. 118, pp. 113901, 2017.
[38] L. Huang, H. Mühlenbernd, X. Li, et al., "Broadband hybrid holographic multiplexing with geometric metasurfaces," *Adv. Mater.*, vol. 27, pp. 6444–6449, 2015.
[39] D. Hu, Y. Lu, Y. Cao, et al., "Laser-splashed three-dimensional plasmonic nanovolcanoes for steganography in angular anisotropy," *ACS Nano*, vol. 12, pp. 9233–9239, 2018.
[40] H. Ren, G. Briere, X. Fang, et al., "Metasurface orbital angular momentum holography," *Nat. Commun.*, vol. 10, pp. 1–8, 2019.
[41] Y. Bao, Y. Yu, H. Xu, et al., "Coherent pixel design of metasurfaces for multidimensional optical control of multiple printing-image switching and encoding," *Adv. Funct. Mater.*, vol. 28, pp. 1805306, 2018.
[42] T. J. Cui, Q. Q. Mei, W. Xiang, Z. Jie, and C. Qiang, "Coding metamaterials, digital metamaterials and programmable metamaterials," *Light. Sci. Appl.*, vol. 3, pp. e218, 2014.
[43] T. J. Cui, L. Shuo, and Z. Lei, "Information metamaterials and metasurfaces," *J. Mater. Chem. C.*, vol. 5, pp. 3644, 2017.
[44] M. A. Al-Joumayly, and B. N. W. Planar, "Microwave lenses using sub-wavelength spatial phase shifters," *IEEE Trans. Antennas Propag.*, vol. 59, pp. 4542–4552, 2011.
[45] R. D. Leonardo, F. Ianni, and G. Ruocco, "Computer generation of optimal holograms for optical trap arrays," *Opt. Express*, vol. 15, pp. 1913–1922, 2007.
[46] F. Zhou, Y. Liu, and W. Cai, "Plasmonic holographic imaging with V-shaped nanoantenna array," *Opt. Express*, vol. 21, pp. 4348, 2013.
[47] L. W. Wu, H. F. Ma, Y. Gou, et al., "High-transmission ultrathin Huygens' metasurface with 360° phase control by using double-layer transmitarray elements," *Phys. Rev. Appl.*, vol. 12, 2019, Art no. 024012.
[48] C. Xue, Q. Lou, and T. Li, "Ultra-compact, broadband Huygens' metasurfaces based on induced magnetism," *Appl. Phys. Express*, vol. 12, 2019, Art no. 072005.

[49] G. Liu, H. J. Wang, J. S. Jiang, F. Xue, and M. Yi, "A High-efficiency transmitarray antenna using double split ring slot elements," *IEEE Antennas Wireless Propag. Lett.*, vol. 14, pp. 1415, 2015.
[50] A. H. Abdelrahman, P. Nayeri, A. Z. Elsherbeni, and F. Yang, "Bandwidth improvement methods of transmitarrays," *IEEE Trans. Antennas Propag.*, vol. 63, pp. 2946, 2015.
[51] H. Chu, J. Qi, S. Xiao, and J. Qiu, "A thin wideband high-spatial-resolution focusing metasurface for near-field passive millimeter-wave imaging," *Appl. Phys. Lett.*, vol. 112, pp. 174101, 2018.
[52] H. Liang, Q. Lin, X. Xie, et al., "Ultrahigh numerical aperture metalens at visible wavelengths," *Nano Lett.*, vol. 18, pp. 4460–4466, 2018.
[53] K. E. Chong, L. Wang, I. Staude, et al., "Efficient polarization-insensitive complex wavefront control using Huygens' metasurfaces based on dielectric resonant meta-atoms," *Acs Photonics*, vol. 3, pp. 514–519, 2016.
[54] L. Wang, S. Kruk, H. Tang, et al., "Grayscale transparent metasurface holograms," *Optica*, vol. 3, pp. 1504–1505, 2016.
[55] A. Arbabi, Y. Horie, A. J. Ball, M. Bagheri, and A. Faraon, "Subwavelength-thick lenses with high numerical apertures and large efficiency based on high-contrast transmitarrays," *Nat. Commun.*, vol. 6, pp. 7069, 2015.
[56] W. Zhao, H. Jiang, B. Liu, et al., "Dielectric Huygens' metasurface for high-efficiency hologram operating in transmission mode," *Sci. Rep.*, vol. 6, pp. 30613, 2016.
[57] S. Zhao, H. Yang, Y. Li, et al., "The influence of atmospheric turbulence on holographic ghost imaging using orbital angular momentum entanglement: simulation and experimental studies," *Opt. Commun.*, vol, 294, pp. 223–228, 2013.
[58] M. Khorasaninejad, W. T. Chen, R. C. Devlin, J. Oh, A. J. Zhu, and F. Capasso, "Metalenses at visible wavelengths: diffraction-limited focusing and subwavelength resolution imaging," *Science*, vol. 352, pp. 1190–1194, 2016.
[59] H. X. Xu, L. Han, Y. Li, et al., "Completely spin-decoupled dual-phase hybrid metasurfaces for arbitrary wavefront control," *ACS Photonics*, vol. 6, pp. 211–220, 2019.
[60] S. N. Burokur, J. P. Daniel, P. Ratajczak, and A. de Lustrac, "Tunable bi-layered metasurface for frequency reconfigurable directive emissions," *Appl. Phys. Lett.*, vol. 97, 2010, Art no. 064101.

Supplementary Material: Supplementary material to this article can be found online at https://doi.org/10.1515/nanoph-2020-0237.